Local dimerization and dedimerization of C_{60} molecules under a tip of scanning tunneling microscope: A first-principles study

Shigeru Tsukamoto[a,*], Masato Nakaya[b,1], Vasile Caciuc[a], Nicolae Atodiresei[a], Tomonobu Nakayama[b,c,*]

[a] *Peter Grünberg Institut & Institute for Advanced Simulation, Forschungszentrum Jülich and JARA, D-52425 Jülich, Germany*
[b] *International Center for Materials Nanoarchitectonics (WPI-MANA), National Institute for Materials Science (NIMS), Tsukuba, Ibaraki 305-0044, Japan*
[c] *Graduate School of Pure and Applied Sciences, University of Tsukuba, Tsukuba, Ibaraki 305-0044, Japan*

Abstract

The local dimerization and dedimerization of C_{60} molecules in a C_{60} thin film using a scanning tunneling microscopy (STM) [M. Nakaya *et al.* Adv. Mater. **22**, 1622 (2010)] are promising techniques for realizing ultradense data storages. However, the detailed mechanism of the reversible topochemical reactions has not been clarified yet. Based on the density functional theory we explain the mechanism in terms of charging and electric-field effects on the molecules. The total-energy calculations reveal that when the C_{60} molecules in the surface layer are negatively charged, the dimerization is promoted and interlayer dimers composed of two C_{60} molecules in different layers are formed

*Corresponding authors
Email addresses: s.tsukamoto@fz-juelich.de (Shigeru Tsukamoto), NAKAYAMA.tomonobu@nims.go.jp (Tomonobu Nakayama)
[1]Present address: Department of Energy Science and Engineering, Nagoya University, Nagoya, Aichi 464-8603, Japan

dominantly over in-plane dimers. When the thin-film surface is positively charged or the inter-layer dimers are exposed to a strong electric field, a C_{60} monomer pair becomes more stable than a C_{60} dimer, and the dedimerization is promoted. These results predict competition between the dimerization and dedimerization of a negatively charged C_{60} binary system in a strong electric field, which is indeed confirmed by our STM experiments. In addition, the dedimerization induced in the electric field is discussed from the viewpoints of the intermolecular donor-acceptor interaction and the charge-dipole relaxation of a C_{60} binary system.

1. Introduction

A C_{60} molecule[1, 2] has a stable spherical-cage structure, and its unique geometry yields the characteristic electronic properties.[3] For instance, it is known that C_{60} molecules condensate to form a fcc-structured molecular crystal[4, 5] or a thin film[6] on a substrate through the van der Waals interaction. C_{60} molecular thin films grown on substrates are considered as a potential platform for building up electronic device elements on/in it, and therefore, have been strenuously investigated so far.[7–16]

In 2010, Nakaya *et al.* experimentally reported that C_{60} molecular thin films can be used as an essential constituent for a topochemical ultradense data storage.[17–20] The most important finding is that one can selectively induce local C_{60} dimerization and dedimerization (decomposition of a C_{60} dimer into two separate C_{60} monomers) in a C_{60} thin film using a scanning tunneling microscopy (STM). Both of the chemical reactions can be induced locally at a molecular level using a STM tip, and the resultant dimers are

confirmed to be nonvolatile at room temperature at least for one week. These facts indicate that the topochemical manipulation of C_{60} molecules can be suitable and applicable to an ultradense data storage. In Ref. [17], two C_{60} molecules are expected to be bound through a [2+2] cycloadditive four-membered ring and form a dumbbell-shaped C_{60} dimer with the D_{2h} point symmetry, because the dumbell-shaped structure is thought to be the most probable one for a C_{60} dimer that two C_{60} monomers coalesce.[21–27] Some other geometries possible for a C_{60} dimer have been so far proposed, *e.g.*, a single-bonded C_{60} dimer and a peanut-shaped one. The former can be excluded, because it is reported to be unstable in charge-neutral condition[25] and to transform easily to a dumbell-shaped dimer.[26] The latter is also excluded, because some of the C–C bonds of C_{60} molecules have to be broken for forming a peanut-shaped C_{60} dimer, suggesting a large energy barrier for the dimerization. In addition, the inter-sphere distance of a peanut-shaped C_{60} dimer is too short, *i.e.*, 8.5–8.7 Å,[27–29] therefore, the local dimerization in a C_{60} molecular crystal/thin film is expected to be obstructed by steric hindrance.

So far, coalescence of C_{60} molecules and formation of a dumbell-shaped C_{60} dimer have been experimentally and theoretically studied,[30–36] while there are few studies that discuss the mechanisms of both dimerization and dedimerization processes together.[37–39] In 2007, Sheka theoretically investigated both of the dimerization and dedimerization from the viewpoint of intermolecular donor-acceptor interaction.[38–40] Referring to a hetero-bimolecular system, *i.e.*, a couple of donor and acceptor molecules, the author points out that the dimerization is promoted when C_{60} molecules are nega-

tively charged, and the dedimerization occurs when C_{60} dimers are positively charged. However, a C_{60} dimer is a homo-bimolecular system composed only of single molecular species. In addition, we cannot ignore the fact that the dedimerization can be induced also when C_{60} dimers are negatively charged, as seen in Figure 2b of Ref. [17]. To the best of our knowledge, the mechanisms of the local C_{60} dimerization and dedimerization reported in Ref. [17] have not been clearly interpreted yet.

In this paper, aiming at providing a consistent interpretation of the local C_{60} dimerization and dedimerization experimentally observed in Ref. [17], we theoretically investigate the total energies of a pair of C_{60} monomers and a dumbell-shaped C_{60} dimer as well as the energy barrier for the dimerization and dedimerization processes within the framework of the density functional theory.[41–43] Since the couple of the chemical reactions occurs locally under a STM tip, we take into account finite external electric fields induced by the STM tip as well as negative/positive charge induced on C_{60} monomer pair/dimer. In addition, we take into account non-uniform distribution of the induced charge to C_{60} spheres, because the dimerization can occur between C_{60} molecules in different layers with different charging states. According to the total energy calculations including the van der Waals interactions,[44–49] we propose theoretical scenarios of the local C_{60} dimerization and dedimerization selectively induced in the STM experiment. We also discuss how the intermolecular donor-acceptor interaction contributes to the reversible chemical reactions based on the first ionization energy and electron affinity of a C_{60} molecule, and compare the contributions from the intermolecular donor-acceptor interaction and the charge-dipole relaxation to the dedimerization

when external electric fields are applied.

2. Methods

2.1. Geometrical optimization

The geometries of the C_{60} binary systems were optimized for both of negatively and positively charged configurations as well as for neutral one using the VASP code,[50–53] a plane-wave-based implementation of the projector-augmented wave (PAW) pseudopotentials proposed by Blöchl.[54, 55] The exchange-correlation interactions were treated through the generalized gradient approximation proposed by Perdew, Burke, and Ernzerhof (GGA-PBE).[56, 57] The dimensions of the computing unit cell used in the geometrical optimization were $L_x = 30$ Å and $L_y = L_z = 20$ Å so as to keep the distance between two C atoms in different computing unit cells more than 13 Å. The geometrical optimization were performed until the forces acting on the C atoms become less than 0.01 eV/Å. The van der Waals interactions were taken into account during the geometrical optimization in a self-consistent manner by employing the nonlocal-correlation-energy functional vdW-DF2[44–46] with the exchange-energy functional developed by Hamada.[58, 59]

2.2. Total energy calculation

Employing the optimized geometries of neutral and charged C_{60} binary systems, the total energies were calculated under application of finite electric fields using the RSPACE code,[60–63] an implementation of the PAW pseudopotentials within the framework of the real-space finite-difference formalism.[64,

65] As far as using the VASP code, it is not enough reliable to compare the total energies between different charged systems due to artificial charge neutralization adopting a uniformly distributed background charge in computations. Since the RSPACE code is capable of adopting isolated boundary conditions, such artificial background charge is not necessary, and therefore, one can compare the total energies between different charged systems using the RSPACE code. To keep consistency of the calculation results obtained by the VASP and RSPACE codes, in the total-energy calculations we also employed GGA-PBE for treating the exchange-correlation interactions. The contribution of the van der Waals interactions to total energy were evaluated through the JuNoLo code,[66] a postprocessing code to calculate the nonlocal correlation energy based on vdW-DF.[47–49] The dimension of the computing unit cell employed in the total-energy calculation were $L_x = 23.7$ Å and $L_y = L_z = 15.6$ Å, and isolated boundary conditions were imposed in all the x, y, and z directions so that external electric fields were able to be applied, as seen in Figs. 1c, 3a, 4b, and 6b.

2.3. STM experiment

All the experiments were carried out in an ultrahigh vacuum chamber with a base pressure of 1.0×10^{-8} Pa, which houses a commercial STM unit (Omicron UHV-STM-1). The C_{60} film was formed on a Si(111)$\sqrt{3}\times\sqrt{3}$R30°-Ag [referred to as Si(111)$\sqrt{3}$-Ag hereafter] surface as a sample.[67] The Si(111)$\sqrt{3}$-Ag surface was prepared by depositing one monolayer (ML) of Ag atoms onto a Si(111)7×7 surface at 600°C. The C_{60} film with a thickness of 5-6 molecular layer was grown by depositing 6 ML of C_{60} molecules onto the Si(111)$\sqrt{3}$-Ag surface at room temperature (RT). C_{60} molecules were

deposited by the thermal evaporation of C_{60} powder (99.95% purity) from a boron-nitride crucible while maintaining a deposition rate of 0.03 ML/min. All the experiments using the STM were carried out using an electrochemically etched Pt-20%Ir tip at RT.

3. Results and discussion

In general, the intermolecular interaction between C_{60} molecules in a C_{60} molecular crystal/thin film is dominated by the weak van der Waals interactions. However, between two C_{60} molecules involved in the formation and decomposition of a C_{60} dimer, a strong chemical interaction must act and be dominant in the intermolecular interactions. As suggested by the STM experiments,[17] only the two C_{60} molecules involved in the chemical reactions are essential, and therefore, we focused only on the two C_{60} molecules for simplicity (see Figs. 1c, 3a, 4b, and 6b). All the calculations on the C_{60} binary systems, *i.e.*, monomer pair, dimer, and intermediate states in the chemical reactions, to be presented in this study are performed within the framework of the density functional theory.[41–43]

Before discussing the dimerization and dedimerization processes under the application of finite sample bias voltages, we should consider the energy diagram of a C_{60} three-layered thin film in a STM without applying any bias voltage, which is schematically drawn in Fig. 1a. Note that for simplicity we ignore the fcc stacking of C_{60} layers in the thin film, and assume a linear stacking of C_{60} molecules in the direction perpendicular to the substrate surface in this study. Since the electronic states of C_{60} molecules are known to form band structures with finite energy dispersion $E_{\rm disp}$ in a monolayer phase,

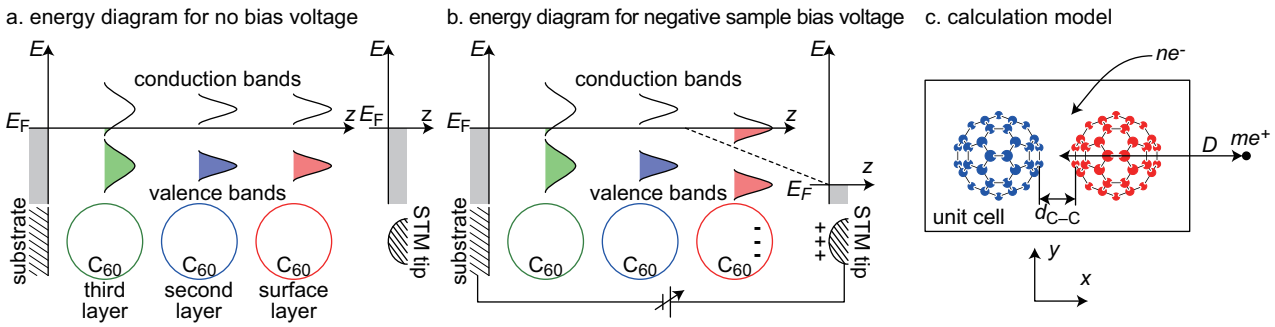

Figure 1: Schematic energy diagram a C_{60} three-layered thin film in a STM setup without application of bias voltage and under application of a finite negative sample bias voltage, and the calculation model of a negatively charged C_{60} binary system. In the panels a and b, occupied states are colored, and E_F represents the Fermi level of either sample and STM-tip sides. The dashed line in the panel b denotes the electric field induced between the STM tip and the surface layer of the thin film. In the panel c, n electrons are added to the computing cell to charge the system negatively, and a $m+$ positive point charge is placed outside it, which models a positively charged STM tip as drawn in the panel b. d_{C-C} denotes the distance between two nearest C atoms in different C_{60} spheres, and D denotes the distance between the point charge and the center of the computing cell.

e.g., $E_{\mathrm{disp}} \approx 0.3$ eV for the conduction and valence bands,[14] the electronic states are drawn not as discrete states but as bands with energy dispersion in the energy diagrams. The energy dispersion of the electronic states of the C_{60} molecular layer attaching to the substrate (referred to as the third layer hereafter) are broadened, because they attach on a metal substrate not only via van der Waals interactions but also via chemical interactions. Such broadening does not occur for the surface and second layers. In addition, it is known that the lowest unoccupied molecular orbital (LUMO) of a C_{60} molecule hybridizes with surface states of a metal substrate and C_{60} molecules attract electrons from the metal due to the electronegativity of the molecules.[15, 16]. This charge transfer causes partial occupation of the conduction band of the C_{60} molecules in the third layer. Consequently, the electronic structure of the C_{60} thin film lowers in energy until the conduction-band bottom of the third layer reaches the Fermi level of the substrate. Here, we assume that although the C_{60} molecules in the third layer are slightly charged negatively, those in the surface and second layers stay neutral, because the energy dispersion of the conduction bands of the surface and second layers is smaller than that of the third layer, as shown in Fig. 1a.

3.1. Dimerization

Now, let us discuss the mechanism of the local dimerization that experimentally occurs when a negative bias voltage is applied to the sample side of a STM (this condition is depicted in Figs. 1b and 6a, and is referred to as negative sample bias voltage hereafter). Firstly, we think about the energy diagram of a C_{60} three-layered thin film under application of negative sample bias voltage, which is schematically drawn in Fig. 1b. When negative bias

voltage is applied to the sample side, positive charge appears on the STM tip and negative charge appears on the C_{60} molecules in the surface layer. Since the conduction band of a C_{60} layer originates from triply degenerated LUMO of a molecule, it is reasonable to suppose that the conduction band is not fully occupied. Since the negative charge shields the electric field induced by the positively charged tip, the external electric field appears only between the surface layer and STM tip, and does not exist inside the C_{60} thin film, as drawn in Fig. 1b. As described in Ref. [17], a C_{60} dimer is formed by two C_{60} molecules in different layers of a C_{60} three-layered thin film, *i.e.*, one of which is in the surface layer and the other in the second layer. Consequently, it is reasonable to suppose that a negatively charged C_{60} molecule in the surface layer and a neutral one in the second layer form a dimer under application of negative sample bias voltage.

Such nonlinear electric field and non-uniform negative-charge distribution to two C_{60} molecules can be reproduced by including an electric field caused by a positively charged STM tip in modeling a C_{60} binary system. More specifically, assuming a positive point charge corresponding to a positively charged STM tip outside the computing unit cell, we add the electrostatic potential induced by the point charge to effective Kohn-Sham potential inside the computing unit cell. Fig. 1c shows the schematic representation of a calculation model of a negatively charged C_{60} binary system used to model the dimerization process. The positive point charge is placed at the position 17 Å away from the center of the computing unit cell along the dimer axis, *i.e.*, $D = 17$ Å in Fig. 1c,[2] and we examine the dimerization process for

[2]We have evaluated the total energies of a C_{60} dimer and a monomer pair with $(m, n) =$

187 the charge indices $(m, n) = (0, 0)$, $(1, 1)$, and $(2, 2)$ (see Fig. 1c for m and
188 n). Note that the optimized geometries of a C_{60} monomer pair and a C_{60}
189 dimer are determined as follows: A C_{60} monomer pair is optimized with
190 keeping the distance between the molecular centers 10 Å. A C_{60} dimer is
191 fully optimized without any restriction. To evaluate the height of the energy
192 barrier for the dimerization/dedimerization process, the geometries of the
193 C_{60} binary systems in the intermediate stages of the chemical reaction are
194 also optimized with keeping the distance between the nearest neighboring
195 C atoms in different C_{60} spheres, $d_{C–C}$, to be 1.84, 2.09, 2.33, and 2.58 Å.
196 Due to this restriction, we cannot exactly find the saddle point of a total-
197 energy surface. Throughout this paper, we refer to the largest total energy
198 among the C_{60} binary systems considered here as the energy-barrier height.
199 Therefore, the barrier heights discussed in this paper may be underestimated.

Fig. 2a shows the total-energy profiles of the negatively charged C_{60} binary systems as a function of $d_{C–C}$, each of which is obtained from the calculations including the external electrostatic potential caused by a counter positive point charge. Note that the total energies ΔE_{tot} are evaluated with respect to that of a C_{60} monomer pair for each (m, n):

$$\Delta E_{tot}(d_{C–C}) = E_{tot}(d_{C–C}) - E_{tot}(\text{monomer pair}). \quad (1)$$

200 In the energy profiles here and later, the obtained data points are connected

$(1, 1)$ for different D. The total energy of the dimer with respect to that of the monomer pair is -0.31, -0.27, and -0.25 eV for $D = 15$, 17, and 19 Å, respectively. Since the energy variation is small, we conclude that small fluctuation of the STM-tip height around $D = 17$ Å does not affect the discussion in this part.

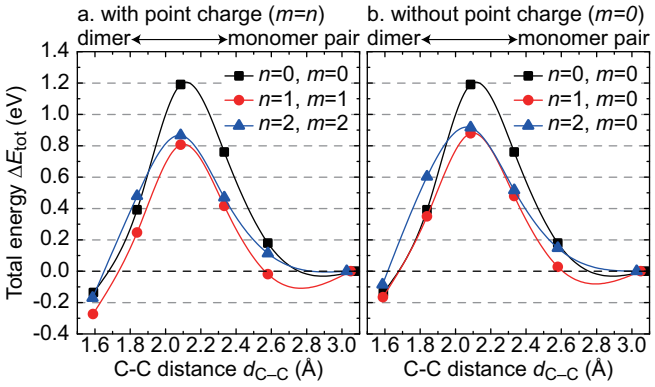

Figure 2: Total-energy profiles of negatively charged C_{60} binary systems as a function of $d_{C–C}$ for different m and n (see Fig. 1c for m and n). The total energies are evaluated with respect to that of a monomer pair for each (m, n). The panel a is for $m = n$ corresponding to the case taking into account a positively charged STM tip, and the panel b is for $m = 0$ corresponding to the case ignoring the effect of a positively charged STM tip.

by a spline interpolation. The difference between the peak value of a spline curve and the highest value of the data points is found not so large, therefore does not change our conclusion. Comparing the total energies of a C_{60} dimer and a C_{60} monomer pair, one can see that the dimer is more stable than the monomer pair by 0.14, 0.27, and 0.17 eV for $n = 0$, 1, and 2, respectively. In addition, the energy barrier for the dimerization decreases from 1.19 eV to 0.81 and 0.87 eV when the C_{60} binary system of $n = 0$ is charged to be $n = 1$ and 2, respectively. These results indicate that the C_{60} dimerization is promoted by charging C_{60} molecules negatively, though a C_{60} dimer is already favorable than a C_{60} monomer pair for $n = 0$.

To elucidate the role of the positively charged STM tip, we calculate the total energies of the negatively charged C_{60} binary systems for $n = 0$, 1, and 2 with keeping $m = 0$, where negative charge added in the computing unit

cell is equally shared by the two C_{60} molecules because of the absence of the external electric field induced by the positive point charge. The total-energies $\Delta E_{\rm tot}$ are evaluated according to Eq. 1, and plotted as a function of $d_{\rm C–C}$ in Fig. 2b. Even excluding the effect from the positive point charge, it is still seen that the dimer is more stable than the monomer pair by 0.14, 0.17, and 0.09 eV for $n = 0$, 1, and 2, respectively. The energy barrier for the dimerization also decreases from 1.19 eV to 0.88 and 0.92 eV when the C_{60} binary system of $n = 0$ is charged to be $n = 1$ and 2, respectively. However, the decrease in the energy barrier in the case including the effect from the point charge is larger than that in the case excluding it. The total-energy difference between the dimer and the monomer pair in the former case is also larger than that in the latter case. These theoretical results can be explained from the fact that Coulomb repulsion between two negatively charged C_{60} molecules is larger than that between a negatively charged C_{60} molecule and a neutral one. Therefore, we conclude that in addition to charging C_{60} molecules, the presence of a positively charged STM tip further promotes the dimerization.

In Ref. [17], the possibility of in-plane dimerization, *i.e.*, dimerization of two negatively charged C_{60} molecules in the surface layer of a C_{60} thin film, is excluded based on the STM experiments. Here, we evaluate the energy barrier for the in-plane dimerization and theoretically investigate this possibility. The calculation model used for this examination under the presence of a positive point charge is drawn in Fig. 3a. The positive point charge representing a positively charged STM tip is placed at the position 12 Å away from the center of the computing unit cell in the y direction perpendicular to

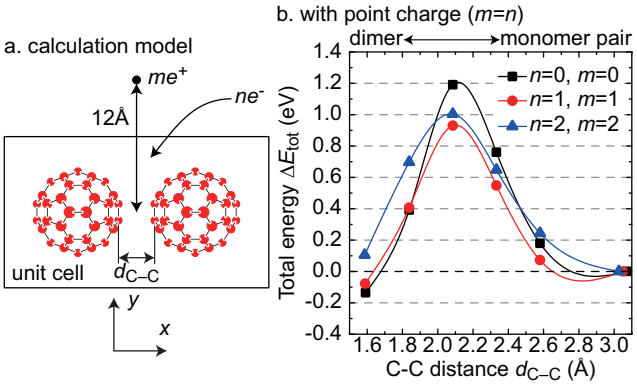

Figure 3: Calculation model used for evaluating the energy barrier for the in-plane dimerization, and the total-energy profiles of negatively charged C_{60} binary systems as a function of $d_{C–C}$ for different m and n (see the model for m and n). In the panel a, n electrons are added to the computing cell, and a $m+$ positive point charge modeling a positively charged STM tip is placed outside it. $d_{C–C}$ represents the distance between the nearest C atoms in different C_{60} spheres. In the panel b, the total energies are evaluated with respect to that of a monomer pair for each (m, n).

the dimer axis. The other computational conditions concerning geometrical optimization and total-energy calculation are the same as the aforementioned ones.

The total energies of the negatively charged C_{60} binary systems in presence of a STM tip modeled by a positive point charge are evaluated according to Eq. 1 for each charge index (m, n) (see Fig. 3a for m and n), and plotted as a function of $d_{C\text{–}C}$ in Fig. 3b. One can see that the energy barrier for the in-plane dimerization decreases from 1.19 eV to 0.93 and 1.00 eV when the C_{60} binary system of $n = 0$ is charged to be $n = 1$ and 2, respectively. However, the energy barrier for the in-plane C_{60} dimerization is still higher than that for the inter-layer C_{60} dimerization shown in Fig. 2a. From Fig. 3b, one can see $\Delta E_{\rm tot}(\text{dimer}) = -0.14$, -0.08, and $+0.10$ eV for $n = 0$, 1, and 2, respectively. By comparing them with those in Fig. 2a, an inter-layer C_{60} dimer is found to be more stable than an in-plane C_{60} dimer, in particular in the case of $n = 2$ the in-plane dimer is even more unstable than the monomer pair. From these results, we conclude that the inter-layer C_{60} dimerization is preferable to the in-plane C_{60} dimerization under a positively charged STM tip.

3.2. Dedimerization at positive sample bias voltage

Here, we discuss the mechanism of the decomposition of a C_{60} dimer that is experimentally observed to occur when a positive bias voltage is applied to the sample side of a STM (this condition id depicted in Fig. 4a, and is referred to as positive sample bias voltage hereafter). As discussed in the preceding subsection as well as seen in Ref. [17], inter-layer C_{60} dimers are formed more dominantly than in-plane C_{60} dimers in a C_{60} thin film under

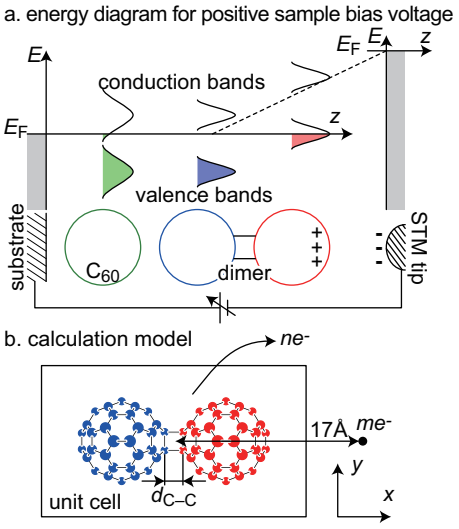

Figure 4: Schematic energy diagram of a C_{60} three-layered thin film under application of finite positive sample bias voltage, and the calculation model of a positively charged C_{60} binary system. In the panel a, occupied states are colored, and E_F in the left and right represents the Fermi level of either sample and STM-tip sides. The dashed line denotes the electric field induced between the STM tip and the surface layer of the thin film. In the panel b, n electrons (ne^-) are removed from the computing cell to charge the system positively, and a $m-$ negative point charge is placed outside it, which models a negatively charged STM tip, as drawn in the panel a. d_{C-C} denotes the bond length between two nearest C atoms in different C_{60} spheres.

a positively charged STM tip. Therefore, we deal with the dedimerization only of the inter-layer dimers hereafter. Since the dedimerization occurs under application of positive sample bias voltage, it is reasonable to suppose that the dimers are positively charged when the dedimerization occurs. A schematic energy diagram of a C_{60} three-layered thin film in the dedimerization process is drawn in Fig. 4a. Since a negatively charged STM tip repels corresponding negative charge from the surface layer of a C_{60} thin film, the

C_{60} spheres in the surface layer are positively charged. Therefore, the positively charged C_{60} spheres shield the electric field induced by a negatively charged STM tip, and an effective electric field appears only between the STM tip and C_{60} spheres in the surface layer, as drawn by the dashed line in Fig. 4a. Consequently, C_{60} spheres in the second layer are expected to remain neutral even when the dedimerization occurs under the application of positive sample bias voltage.

Such nonlinear electric field and non-uniform positive-charge distribution in the two C_{60} spheres can be reproduced in the same way introduced in the preceding subsection, *i.e.*, assuming a negative point charge corresponding to a negatively charged STM tip outside a computing unit cell, we add electrostatic potential induced by the point charge to effective Kohn-Sham potential inside the computing unit cell. Fig. 4b shows the schematic representation of a calculation model of a positively charged C_{60} binary system used to examine the dedimerization process. The negative point charge is placed at the position 17 Å away from the center of the computing unit cell along the dimer axis. We examine the dedimerization process of a positively charged C_{60} binary system with an external electric field induced by the negative point charge, *i.e.*, $(m, n) = (0, 0)$, $(1, 1)$, and $(2, 2)$, and without the external electric field, *i.e.*, $(m, n) = (0, 0)$, $(0, 1)$, and $(0, 2)$ The optimized geometries and total energies of the C_{60} monomer pair, dimer, and intermediate binary systems considered in this subsection are obtained in the same manner as mentioned in the preceding subsection.

Figs. 5a and 5b show the total-energy profiles of the positively charged C_{60} binary systems as a function of $d_{C–C}$, which are obtained from the cal-

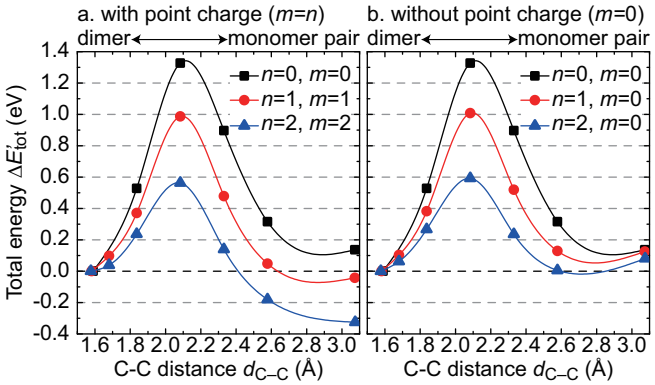

Figure 5: Total-energy profiles of positively charged C_{60} binary systems as a function of $d_{C–C}$ for different m and n (see Fig. 4b for m and n). The total energies are evaluated with respect to that of a dimer for each (m, n). The panel a is for $m = n$ corresponding to the case taking into account a negatively charged STM tip, and the panel b is for $m = 0$ corresponding to the case excluding the effect of a negatively charged STM tip.

culations including and excluding external electrostatic potential caused by a negatively charged STM tip modeled by a negative point charge, respectively. Note that the total energies are evaluated with respect to that of a C_{60} dimer for each (m, n):

$$\Delta E'_{\rm tot}(d_{\rm C–C}) = E_{\rm tot}(d_{\rm C–C}) - E_{\rm tot}(\text{dimer}). \tag{2}$$

One can clearly see in Fig. 5a that the C_{60} monomer pair has the total energy lower than a C_{60} dimer by 0.04 eV for $n = 1$ and 0.33 eV for $n = 2$, while the neutral C_{60} monomer pair has the total energy higher than a neutral C_{60} dimer by 0.14 eV. On the other hand, in Fig. 5b a dimer is found to have the lowest energy in the total-energy profile for any n, *i.e.*, $\Delta E'_{\rm tot}(d_{\rm C–C}) > 0$ for any $d_{\rm C–C}$ in the right-hand side of the energy barrier. These results lead the following conclusion: Only in presence of a negatively charged STM tip, a

positively charged C_{60} monomer pair is more stable than a dimer, otherwise the dimer is preferable to the monomer pair. The energy barrier between the dimer and the monomer pair significantly decreases regardless of the presence of the negatively charged STM tip, *i.e.*, when increasing n from 0 to 1 (2) it decreases from 1.33 eV to 0.99 (0.56) and 1.01 (0.59) eV in Figs. 5a and 5b, respectively. Consequently, we find that the dedimerization of an inter-layer C_{60} dimer is promoted by charging the dimer positively, and an external electric field caused by a negatively charged STM tip must be applied to the C_{60} binary system.

3.3. Dedimerization at negative sample bias voltage

In Figure 2b of Ref. [17], the dedimerization is observed to occur at a negative sample bias voltage as well as at a positive one, and its probability is non-negligible. Here, we discuss the mechanism of the dedimerization of inter-layer C_{60} dimers at negative sample bias voltage. Comparing Figure 2a and 2b of Ref. [17], one can see that the dedimerization occurs at a negative sample bias voltage smaller than that triggering the dimerization. Therefore, we suppose an energy diagram of a C_{60} three-layered thin film in a STM, as schematically drawn in Fig. 6a. Due to application of a negative sample bias voltage, the electronic structure of the C_{60} surface layer lowers in energy. The energy shift is, however, not as large as the case of the dimerization process, which is shown in Fig. 1b. The conduction band of the surface layer may remain unoccupied or be slightly occupied, because of the finite energy gap

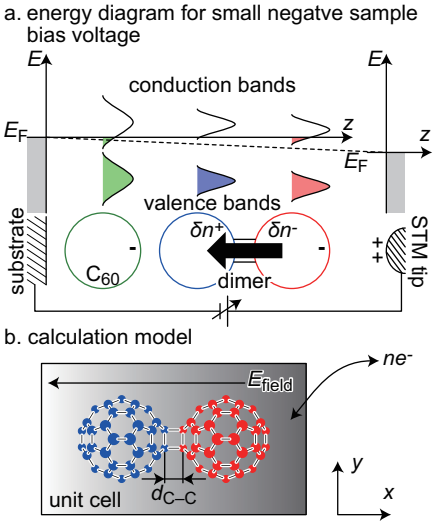

Figure 6: Schematic energy diagram of a C_{60} three-layered thin film under the application of small negative sample bias voltage, and the calculation model of a neutral/charged C_{60} binary system exposed to a uniform external electric field E_{field}. In the panel a, occupied states are colored, and E_{F} in the left and right represents the Fermi level of either sample and STM-tip sides. The dashed line denotes the electric field induced between the STM tip and the third layer of the thin film. In the panel b, n electrons are added/removed to/from the computing cell to charge the system negatively/positively. $d_{\mathrm{C–C}}$ denotes the bond length between two nearest C atoms in different C_{60} spheres, and E_{field} is applied along the dimer axis.

between the valence and conduction bands.[3] The induced negative charge is supposed too little to screen the C_{60} dimers from the electric field induced by a positively charged STM tip, as seen in Fig. 6a. Therefore, the dimers are exposed to an electric field and it has a charge polarization[68] as indicated by the thick arrow in Fig. 6a. To screen the substrate from the electric field, additional negative charge is supposed to be induced in the third layer, as drawn in Fig. 6a. When negative sample bias voltage increases to induce more negative charge on the surface of the C_{60} thin film, the charge dipole disappears and the electric field inside the thin film vanishes. Because of this, the dedimerization is expected not to occur any more at large negative sample bias voltage. Consequently, we expect that the dedimerization observed at negative sample bias voltage is driven by an external electric field imposed on neutral or slightly charged dimers.

To evaluate the energy barrier for the dedimerization of such C_{60} dimer exposed to external electric fields, we employ the calculation model drawn in Fig. 6b, and calculate the total energies of the C_{60} binary systems for different $d_{\mathrm{C\text{–}C}}$. Since we assume to apply a uniform electric field E_{field} in the direction of the dimer axis (the x direction), electrostatic potential $V_{\mathrm{field}}(\boldsymbol{r}) = -E_{\mathrm{field}}x$ is added to an effective Kohn-Sham potential, where $\boldsymbol{r} = (x, y, z)$. Note that the origin of the x coordinate is set at the center of the computing unit cell in this study.

As discussed in the last two subsections, a neutral C_{60} dimer is more

[3] Our calculation reveals that an isolated C_{60} dimer has the HOMO-LUMO gap of ≈ 1.4 eV. Therefore, we assume that a molecular layer composed of C_{60} dimers also has a finite energy gap between the valence and conduction bands around 1.4 eV.

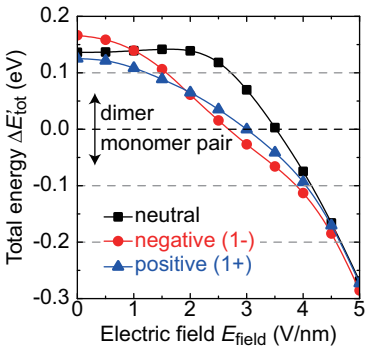

Figure 7: Total-energy profiles of neutral, negatively, and positively charged C_{60} monomer pairs as a function of $E_{\rm field}$. The total energies are evaluated with respect to that of the corresponding dimer for each charged state.

stable than a neutral C_{60} monomer pair without taking into account finite external electric fields. Therefore, before examining the energy barrier for the dedimerization, we firstly examine and compare the total energies of the C_{60} monomer pair and dimer for each of different external electric fields $E_{\rm field}$. Fig. 7 shows the total energy of a neutral/charged C_{60} monomer pair with respect to that of the corresponding dimer as a function of $E_{\rm field}$, which is evaluated using Eq. 2. It is seen that when the C_{60} binary system is neutral, $\Delta E'_{\rm tot}$ is positive up to $E_{\rm field} = 3.5$ V/nm and becomes negative for $E > 3.5$ V/nm. This indicates that a neutral C_{60} monomer pair is favorable as compared to a neutral C_{60} dimer for $E > 3.5$ V/nm, though the dimer is more stable than the monomer pair for the smaller electric fields. The threshold electric field is ≈ 2.7 V/nm for a negatively charged C_{60} binary system and is ≈ 3.0 V/nm for a positively charged one. These values are apparently smaller than that for a neutral C_{60} binary system. Consequently, the dedimerization is found to be promoted when a C_{60} dimer is charged

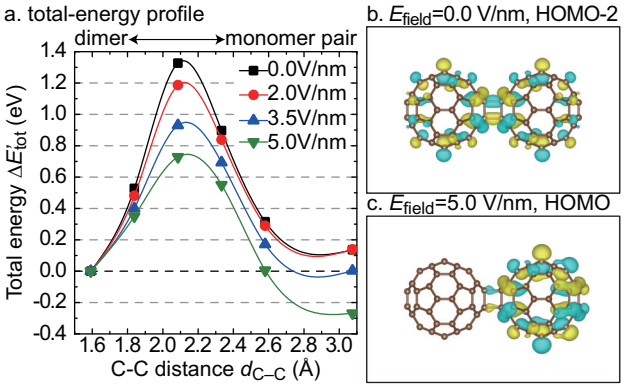

Figure 8: Total-energy profiles of neutral C_{60} binary systems as a function of $d_{C–C}$ for different E_{field}, and the wave functions of the bonding states between two C_{60} spheres. The total energies are evaluated with respect to that of a dimer for each E_{field}. The panels b and c show the second-highest occupied molecular orbital (HOMO-2) and the highest occupied molecular orbital (HOMO) of a dimer in $E_{field} = 0.0$ and 5.0 V/nm, respectively.

either negatively or positively, as far as an electric field inside the C_{60} thin film is not completely shielded. Moreover, the calculations also indicate that the dedimerization of a positively charged C_{60} dimer needs stronger electric field than that of a negatively charged one.

Now let us examine the energy barrier for the dedimerization of a neutral C_{60} dimer under application of uniform external electric fields. Fig. 8a shows the total-energy profiles of the C_{60} binary systems as a function of $d_{C–C}$ for $E_{field} = 0.0$, 2.0, 3.5, and 5.0 V/nm. Note that the total energies are evaluated using Eq. 2 for each E_{field}. One can see that by increasing E_{field} the barrier height for the dedimerization of the neutral C_{60} dimer decreases, *i.e.*, the barrier heights for $E_{field} = 0.0$, 2.0, 3.5, and 5.0 V/nm are 1.33, 1.19, 0.93, and 0.73 eV, respectively. Interestingly, when E_{field} is increased from 0.0 V/nm to 2.0 V/nm, $\Delta E'_{tot}$ hardly changes, but the barrier height nevertheless

changes by 0.14 eV. As increasing E_{field}, the energy barrier keeps decreasing. This reduction of the energy barrier can be understood from the spatial distributions of electronic states: The electronic state with a bonding character between the two C_{60} spheres in a dimer is found to delocalize over the whole dimer for $E_{\text{field}} = 0.0$ V/nm as seen in Fig. 8b, however, it localizes at one of the spheres for $E_{\text{field}} = 5.0$ V/nm as seen in Fig. 8c. This localization is obviously caused by the application of the external electric field. Because of the localization of the bonding state, the two spheres in $E_{\text{field}} = 5.0$ V/nm are not bound to each other as strong as those in $E_{\text{field}} = 0.0$ V/nm. Consequently, we conclude from our calculations that the dedimerization of a C_{60} dimer is promoted under the application of a strong external electric field.

The preceding discussion can be applied also to the case of a small positive sample bias voltage. Under the application of a small positive sample bias voltage, C_{60} dimers are remain neutral or positively charged slightly. Analogous to the preceding discussion, it is expected that the positive charge induced is not much enough to completely shield the electric field induced by a negatively charged STM tip. Therefore, the dimers can be exposed to a finite electric field under the application of a small positive sample bias voltage. In Figure 2a of Ref. [17], the threshold bias voltage for the dimerization reads -2.0 V and the dimerization is suddenly triggered off. On the other hand, according to the STM experiments shown in Figure 2b of Ref. [17], although the threshold bias voltage for the dedimerization is read to be +3.0 V, the dedimerization slightly occurs at positive bias voltage smaller than the threshold value. We suppose that this dedimerization observed at the small positive bias voltage is also driven by the application of an external

electric field to neutral or slightly positively charged C_{60} dimers. The experimental observation that the dedimerization probability for positive sample bias is smaller than that for negative sample bias voltage (see Figure 2b of Ref. [17]) can be understood as follows: According to Fig. 7, the threshold electric field where a C_{60} monomer pair becomes more stable than a C_{60} dimer is ~ 2.7 V/nm for a negatively charged binary system and ~ 3.0 V/nm for a positively charged one. This indicates that the dedimerization driven by the external electric fields is more probable for a negative sample bias voltage than for a positive sample bias voltage.

3.4. Hinderance of dimerization by external field

Fig. 7 can be also used to explain the experimental result that the dimerization process is suppressed under application of a strong electric field. Fig. 9 shows a couple of STM images taken at the sample bias voltage $V_{\mathrm{s}} = +1.0$ V and current set point $I_{\mathrm{t}} = 25$ pA after dimerization experiments on a multilayered (> 5) C_{60} thin film. The dimerization is carried out by scanning the square areas enclosed by the dashed lines with $V_{\mathrm{s}} = -2.5$ V and $I_{\mathrm{t}} = 0.08$ nA for Fig. 9a, and $I_{\mathrm{t}} = 40$ nA for Fig. 9b. According to the I_{t} values, one can see that the tip–sample distance for the latter is much shorter than that for the former, and hence, the tip-induced electric field for the latter is stronger than that for the former. Therefore, it is seen that when a weak electric field is applied for the dimerization process, coalesced C_{60} molecules are formed in the scanned area. On the other hand, when a strong electric field is applied, they are mainly formed in the surroundings of the scanned area and C_{60} monomers remain to be in the majority inside the scanned area. At a weak electric-field regime, dot-like features, ultimately single-molecule-level

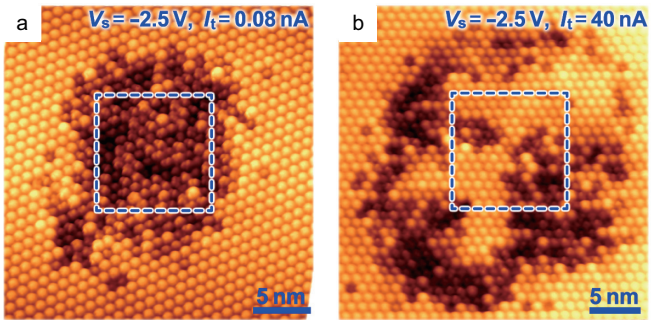

Figure 9: STM images of a multi-layered (> 5) C_{60} thin film after dimerization experiments. The experiments are carried out by scanning the square areas enclosed by the dashed lines with a sample bias voltage $V_s = -2.5$ V. The current set points during the experiment are $I_t = 0.08$ nA and 40 nA for the panels a and b, respectively. Both images are taken at $V_s = +1.0$ V and $I_t = 25$ pA.

features, appear as previously reported in Ref. [17]. However, increasing the applied electric field always results in the enlargement of the dot size and finally in the formation of ring patterns as shown in Fig. 9. The voltage or current setting to induce such a ring-pattern formation depends on a condition of the STM tip such as curvature and local density of states (LDOS) of the tip apex because such a condition readily changes the spatial distribution and the strength of the electric field around the tip. We suppose that the difference in the dimerization is attributed to poor electronic screening[69–71] at the surface of the C_{60} thin film, which often occurs at the surface of a semiconducting/insulating substrate underneath a STM tip. Because of the poor electronic screening, the strong electric field induced by a STM tip is not completely shielded and C_{60} molecules in the thin film are exposed to a stronger electric field. Fig. 7 shows that when a C_{60} binary system is exposed to a strong electric field it prefers to form a monomer pair instead of a dimer.

Therefore, inside the scanned area shown in Fig. 9b the unshielded electric field hinders C_{60} monomers from coalescing, while in the surroundings the coalescence occurs because the unshielded electric field is not strong enough to suppress it. In the same way, the formation of coalesced C_{60} molecules inside the scanned area shown in Fig. 9a can be also understood.

3.5. Donor-acceptor interaction & charge-dipole relaxation

As one can intuitively expect, a neutral C_{60} binary system under application of finite electric fields (see Fig. 6a) has a charge dipole, in which one C_{60} sphere is negatively charged, and the other positively, *i.e.*, the former works as an electron acceptor and the latter as an electron donor. Sheka theoretically studied the C_{60} dimerization and dedimerization from the viewpoint of the intermolecular donor-acceptor interaction.[38–40] On the other hand, one can also suppose that the charge dipole may be relaxed when the oppositely charged two C_{60} spheres are separated from each other along the direction of E_{field}. In the rest of this section, we examine the role of the intermolecular donor-acceptor interaction in the local C_{60} dimerization and dedimerization induced by a STM tip, and discuss about the degree of the contribution of the intermolecular donor-acceptor interaction to the chemical reactions in comparison to that of the charge-dipole relaxation. According to the Sheka's study, the only essential parameter dominating the energy diagrams of the reversible chemical reactions is the energy difference between the first ionization energy (E_{ie}) and electron affinity (E_{ea}) of a neutral C_{60} molecule, *i.e.*, $E_{\mathrm{ie}} - E_{\mathrm{ea}}$. In this study, E_{ie} and E_{ea} are evaluated from the

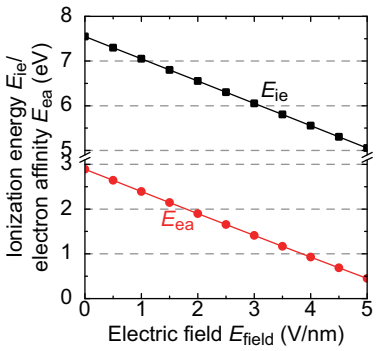

Figure 10: The first ionization energy ($E_{\rm ie}$) and electron affinity ($E_{\rm ea}$) of an isolated C_{60} molecule as a function of $E_{\rm field}$.

total energies, $E_{\rm tot}$, of charged and neutral C_{60} molecules, as

$$E_{\rm ie} = E_{\rm tot}(C_{60}^{1+}) - E_{\rm tot}(C_{60}) \quad (3)$$

$$E_{\rm ea} = E_{\rm tot}(C_{60}) - E_{\rm tot}(C_{60}^{1-}), \quad (4)$$

respectively. In Fig. 10, $E_{\rm ie}$ and $E_{\rm ea}$ are plotted as a function of $E_{\rm field}$. It is confirmed that $E_{\rm ie}$ and $E_{\rm ea}$ for $E_{\rm field} = 0.0$ V/nm are in good agreement with previous experimental works[72–74] and theoretical ones.[75–78] Each of $E_{\rm ie}$ and $E_{\rm ea}$ monotonically decreases with a uniform gradient as increasing $E_{\rm field}$. Since the gradients of $E_{\rm ie}$ and $E_{\rm ea}$ profiles are almost identical to each other, $E_{\rm ie} - E_{\rm ea}$ is nearly constant in the range of $E_{\rm field}$ considered here. More exactly, $E_{\rm ie} - E_{\rm ea}$ slightly decreases only by 0.06 eV when $E_{\rm field}$ increases from 0.0 V/nm to 5.0 V/nm. This change in $E_{\rm ie} - E_{\rm ea}$ is too small to explain the change in $\Delta E_{\rm tot}$ from $E = 0.0$ V/nm to 5.0 V/nm, *i.e.*, -0.40 eV as seen in Fig. 7.

The dipole-relaxation energy is evaluated through the difference in the dipole energies of a C_{60} monomer pair and a C_{60} dimer in an external electric

field, $\Delta E_{\rm dip}$, which is plotted in Fig. 11 as a function of $E_{\rm field}$. In this study, $\Delta E_{\rm dip}$ is defined as

$$\Delta E_{\rm dip} = E_{\rm dip}(\text{monomer pair}) - E_{\rm dip}(\text{dimer}), \tag{5}$$

where the first and second terms in the right-hand side represent the dipole energies of a monomer pair and a dimer, respectively. They are evaluated as

$$E_{\rm dip} = \int V_{\rm field}(\boldsymbol{r})\rho(\boldsymbol{r})\mathrm{d}\boldsymbol{r} - \sum_i V_{\rm field}(\boldsymbol{r}_i)Z_i, \tag{6}$$

where $V_{\rm field}(\boldsymbol{r})$ and Z_i represent the electrostatic potential generated by an external electric field at a position $\boldsymbol{r}$ and the positive charge of ith ion core at $\boldsymbol{r}_i$, respectively. One can see from Fig. 11 that $\Delta E_{\rm dip}$ is negligibly small up to $E_{\rm field} = 2.5$ V/nm, and it decreases to -1.13 eV when increasing $E_{\rm field}$ from 2.0 V/nm to 5.0 V/nm. This energy variation is more significant than that of $E_{\rm ie} - E_{\rm ea}$, and the behavior of $\Delta E_{\rm dip}$ is consistent with that of $\Delta E'_{\rm tot}$ shown in Fig. 7. Therefore, we conclude that the relaxation of a charge dipole in a neutral C_{60} binary system under an external electric field plays a more important role in the dedimerization process than the intermolecular donor-acceptor interaction.

As seen in Fig. 11, the dipole-energy relaxation on the dedimerization mainly occurs for $E_{\rm field} > 2.5$ V/nm. This behavior of $\Delta E_{\rm dip}$ can be explained based on the dipole charge δn. In Fig. 11, δn of a C_{60} monomer pair and of a C_{60} dimer are also drawn as a function of $E_{\rm field}$. For $E_{\rm field} < 2.5$ V/nm, δn of a C_{60} monomer pair is smaller than that of a C_{60} dimer, indicating that when two C_{60} spheres of a dimer separate from each other along the electric field, a part of negative charge moves against the electric field

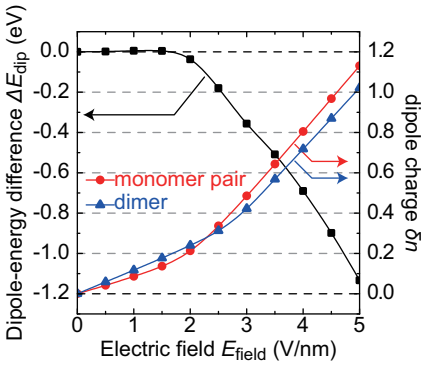

Figure 11: Dipole-energy of a neutral C_{60} monomer pair with respect to that a C_{60} dimer for different $E_{\rm field}$, and dipole charge induced in the monomer pair and dimer under application of different $E_{\rm field}$.

to reduce δn. Therefore, the energy relaxation on the dedimerization is negligible for $E_{\rm field} < 2.5$ V/nm. On the other hand, for $E_{\rm field} > 2.5$ V/nm, additional negative charge moves along the electric field to increase δn during the dedimerization process. This increase in δn increases in electrostatic energy for a C_{60} monomer pair, and therefore, a C_{60} monomer pair becomes more stable than a C_{60} dimer under application of a large external electric field.

4. Conclusion

Aiming at theoretically understanding the mechanisms of the local C_{60} dimerization and dedimerization induced in a C_{60} three-layered thin film using STM, we compared the total energies of a C_{60} monomer pair and a C_{60} dimer, and discussed the energy barriers for the dimerization and dedimerization processes based on the first-principles calculations including the van der Waals interactions within the framework of the density functional the-

ory. As a result of the total-energy calculations, it was found that when C_{60} molecules in the surface layer of a C_{60} thin film is negatively charged and the tip-induced electric field is completely shielded, the inter-layer dimerization is promoted. On the other hand, when the C_{60} molecules are positively charged and the tip-induced electric field is completely shielded, the dedimerization of the inter-layer dimers is present. We studied not only the charging effect mentioned above but also the the electric-field effect in the reversible chemical reactions, which emerges when a tip-induced electric field is incompletely shielded. The total-energy calculations of a C_{60} binary system under external electric fields revealed that the C_{60} binary system prefers being a dimer for weak electric fields, while it prefers to be a monomer pair for strong electric fields. Note that the electric-field effect does not depend on the polarity of sample bias voltage.

According to the calculation results, we developed scenarios to interpret the reversible chemical reactions observed in Ref. [17]. When a very small negative sample bias, *e.g.*, $|V_{\rm s}| < 1$ V in Figure 2 of Ref. [17], is applied, C_{60} molecules in the surface layer would remain neutral and the C_{60} thin film is exposed to a weak electric field. According to Fig. 8, the energy barrier for the dimerization of a neutral C_{60} monomer pair under a weak electric field is still as high as that for the in-plane dimerization (see Fig. 3b), and the energy barrier for the dedimerization of a neutral C_{60} dimer is even higher. Consequently, none of the dimerization and dedimerization occurs when a very small negative sample bias is applied, as well as the case of no electric field. When the negative sample bias voltage is increased so far as the poor electronic screening occurs, a C_{60} monomer pair becomes more

stable than a C_{60} dimer as discussed in Fig. 7 and the energy barrier for the dedimerization decreases as shown in Fig. 8, resulting in promoting the dedimerization. As increasing the negative sample bias voltage further, C_{60} molecules in the surface layer is negatively charged enough to shielded the electric field inside the C_{60} thin film. Then, the charging effect takes over the tip-induced electric-field one, and the dimerization occurs.

In the case of application of positive sample bias voltage, the dedimerization shown in Figure 2 of Ref. [17] is supposed to be caused by both electric-field and charging effects. When a small positive sample bias voltage is applied, C_{60} dimers in a C_{60} thin film are not or slightly charged. Due to poor electronic screening, the C_{60} dimers are exposed to an external electric field and the dedimerization is promoted when the electric field penetrating into the C_{60} thin film becomes strong. However, since a positively charged C_{60} dimer requires stronger electric field for dedimerization than a negatively charged one, as shown in Fig. 7, the dedimerization probability observed in Figure 2 of Ref. [17] is very small. As increasing the positive sample bias voltage further, C_{60} dimers formed in a C_{60} thin film are positively charged enough to shielded the electric field inside the thin film. Then, the charging effect becomes dominant over the electric-field one in the dedimerization process under a positively charged STM tip.

Additionally, we revealed that the dimerization occurs to form mainly a inter-layer C_{60} dimer made of two C_{60} monomers in surface and second layers. Based on the poor electronic screening of a tip-induced electric field, we gave a plausible interpretation to the experimental observation that the dimerization is hindered by application of a strong tip-induced electric field. More-

over, we discussed the contributions of the intermolecular donor-acceptor interaction and charge-dipole relaxation to the reversible chemical reactions, and revealed that the charge-dipole relaxation contributes more than the intermolecular donor-acceptor interaction.

Acknowledgement

S. T., V. C., and N. A. acknowledge the financial support from Deutsche Forschungsgemeinschaft (DFG, German Research Foundation) through the Project number 641366 (AT 109/5-1) and the Project number 277146847 - Collaborative Research Center SFB 1238 (project C01). The calculations presented in this paper are partly executed on the supercomputer JURECA at Jülich Supercomputing Center of Forschungszentrum Jülich using the computing time granted through JARA-HPC.

References

[1] H. W. Kroto, C_{60}: Buckminsterfullerene, The celestial sphere that fell to earth, Angew. Chem., Int. Ed. Engl. 31 (2) (1992) 111–129. doi:10.1002/anie.199201113.

[2] H. W. Kroto, J. R. Heath, S. C. Obrien, R. F. Curl, R. E. Smalley, C_{60}: Buckminsterfullerene, Nature 318 (6042) (1985) 162–163. doi:10.1038/318162a0.

[3] M. S. Dresselhaus, G. Dresselhaus, P. Eklund, Science of Fullerenes and Carbon Nanotubes, Academic Press, San Diego, 1996. doi:10.1016/B978-0-12-221820-0.X5000-X.

[4] W. Krätschmer, L. D. Lamb, K. Fostiropoulos, D. R. Huffman, Solid C_{60}: a new form of carbon, Nature 347 (6291) (1990) 354–358. doi:10.1038/347354a0.

[5] S. Saito, A. Oshiyama, Cohesive mechanism and energy bands of solid C_{60}, Phys. Rev. Lett. 66 (20) (1991) 2637–2640. doi:10.1103/PhysRevLett.66.2637.

[6] Y. Z. Li, J. C. Patrin, M. Chander, J. H. Weaver, L. P. F. Chibante, R. E. Smalley, Ordered overlayers of C_{60} on GaAs(110) studied with scanning tunneling microscopy, Science 252 (5005) (1991) 547–548. doi:10.1126/science.252.5005.547.

[7] M. Paßens, V. Caciuc, N. Atodiresei, M. Feuerbacher, M. Moors, R. E. Dunin-Borkowski, et al., Interface-driven formation of a two-dimensional dodecagonal fullerene quasicrystal, Nat. Commun. 8 (2017) 15367. doi:10.1038/ncomms15367.

[8] R. J. Wilson, G. Meijer, D. S. Bethune, R. D. Johnson, D. D. Chambliss, M. S. de Vries, et al., Imaging C_{60} clusters on a surface using a scanning tunnelling microscope, Nature 348 (6302) (1990) 621–622. doi:10.1038/348621a0.

[9] A. M. Rao, P. Zhou, K.-A. Wang, G. T. Hager, J. M. Holden, Y. Wang, et al., Photoinduced polymerization of solid C_{60} films, Science 259 (5097) (1993) 955–957. doi:10.1126/science.259.5097.955.

[10] M. Núñez-Regueiro, L. Marques, J. L. Hodeau, O. Béthoux, M. Perroux,

Polymerized fullerite structures, Phys. Rev. Lett. 74 (2) (1995) 278–281. doi:10.1103/PhysRevLett.74.278.

[11] M. Nakaya, Y. Okawa, C. Joachim, M. Aono, T. Nakayama, Nano-junction between fullerene and one-dimensional conductive polymer on solid surfaces, ACS Nano 8 (12) (2014) 12259–12264. doi:10.1021/nn504275b.

[12] M. Nakaya, Y. Kuwahara, M. Aono, T. Nakayama, Reversibility-controlled single molecular level chemical reaction in a C_{60} monolayer via ionization induced by scanning transmission microscopy, Small 4 (5) (2008) 538–541. doi:10.1002/smll.200701242.

[13] S. Tsukamoto, T. Nakayama, M. Aono, Stable molecular orientations of a C_{60} dimer in a photoinduced dimer row, Carbon 45 (6) (2007) 1261–1266. doi:10.1016/j.carbon.2007.01.023.

[14] L. A. Chernozatonskii, A. G. Kvashnin, P. B. Sorokin, Heterostructures based on graphene and MoS_2 layers decorated by C_{60} fullerenes, Nanotechnology 27 (36) (2016) 365201. doi:10.1088/0957-4484/27/36/365201.

[15] A. Tamai, A. P. Seitsonen, F. Baumberger, M. Hengsberger, Z.-X. Shen, T. Greber, et al., Electronic structure at the C_{60}/metal interface: An angle-resolved photoemission and first-principles study, Phys. Rev. B: Condens. Matter Mater. Phys. 77 (7) (2008) 075134. doi:10.1103/PhysRevB.77.075134.

[16] S. Modesti, S. Cerasari, P. Rudolf, Determination of charge states of C_{60} adsorbed on metal surfaces, Phys. Rev. Lett. 71 (15) (1993) 2469–2472. doi:10.1103/PhysRevLett.71.2469.

[17] M. Nakaya, S. Tsukamoto, Y. Kuwahara, M. Aono, T. Nakayama, Molecular scale control of unbound and bound C_{60} for topochemical ultradense data storage in an ultrathin C_{60} film, Adv. Mater. (Weinheim, Ger.) 22 (14) (2010) 1622–1625. doi:10.1002/adma.200902960.

[18] M. Nakaya, M. Aono, T. Nakayama, Molecular-scale size tuning of covalently bound assembly of C_{60} molecules, ACS Nano 5 (10) (2011) 7830–7837. doi:10.1021/nn201869g.

[19] M. Nakaya, M. Aono, T. Nakayama, Ultrahigh-density data storage into thin films of fullerene molecules, Jpn. J. Appl. Phys. 55 (11) (2016) 1102B4. doi:10.7567/jjap.55.1102b4.

[20] M. Nakaya, Y. Kuwahara, M. Aono, T. Nakayama, Nanoscale control of reversible chemical reaction between fullerene C_{60} molecules using scanning tunneling microscope, J. Nanosci. Nanotechnol. 11 (4) (2011) 2829–2835. doi:10.1166/jnn.2011.3898.

[21] G.-W. Wang, K. Komatsu, Y. Murata, M. Shiro, Synthesis and X-ray structure of dumb-bell-shaped C_{120}, Nature 387 (6633) (1997) 583–586. doi:10.1038/42439.

[22] G. E. Scuseria, What is the lowest-energy isomer of the C_{60} dimer?, Chem. Phys. Lett. 257 (5) (1996) 583–586. doi:10.1016/0009-2614(96)00599-4.

[23] P. W. Fowler, D. Mitchell, R. Taylor, G. Seifert, Structures and energetics of dimeric fullerene and fullerene oxide derivatives, J. Chem. Soc., Perkin Trans. 2 (1972-1999) (10) (1997) 1901–1905. doi:10.1039/A703836D.

[24] J. Fagerström, S. Stafström, Formation of C_{60} dimers: A theoretical study of electronic structure and optical absorption, Phys. Rev. B: Condens. Matter Mater. Phys. 53 (19) (1996) 13150–13158. doi:10.1103/PhysRevB.53.13150.

[25] N. Matsuzawa, M. Ata, D. A. Dixon, G. Fitzgerald, Dimerization of C_{60}: The formation of dumbbell-shaped C_{120}, J. Phys. Chem. 98 (10) (1994) 2555–2563. doi:10.1021/j100061a009.

[26] M. Menon, K. R. Subbaswamy, M. Sawtarie, Structure and properties of C_{60} dimers by generalized tight-binding molecular dynamics, Phys. Rev. B: Condens. Matter Mater. Phys. 49 (19) (1994) 13966–13969. doi:10.1103/PhysRevB.49.13966.

[27] D. L. Strout, R. L. Murry, C. Xu, W. C. Eckhoff, G. K. Odom, G. E. Scuseria, A theoretical study of buckminsterfullerene reaction products: C_{60}+C_{60}, Chem. Phys. Lett. 214 (6) (1993) 576–582. doi:10.1016/0009-2614(93)85686-I.

[28] K. Esfarjani, Y. Hashi, J. Onoe, K. Takeuchi, Y. Kawazoe, Vibrational modes and ir analysis of neutral photopolymerized C_{60} dimers, Phys. Rev. B: Condens. Matter Mater. Phys. 57 (1) (1998) 223–229. doi:10.1103/PhysRevB.57.223.

[29] S. Tsukamoto, T. Nakayama, First-principles electronic structure calculations for peanut-shaped C_{120} molecules, Sci. Technol. Adv. Mater. 5 (5–6) (2004) 617–620. doi:10.1016/j.stam.2004.02.026.

[30] S. Pekker, A. Jánossy, L. Mihaly, O. Chauvet, M. Carrard, L. Forró, Single-crystalline $(KC_{60})_n$: A conducting linear alkali fulleride polymer, Science 265 (5175) (1994) 1077–1078. doi:10.1126/science.265.5175.1077.

[31] Y. Iwasa, T. Arima, R. M. Fleming, T. Siegrist, O. Zhou, R. C. Haddon, et al., New phases of C_{60} synthesized at high pressure, Science 264 (5165) (1994) 1570–1572. doi:10.1126/science.264.5165.1570.

[32] M. Nakaya, M. Aono, T. Nakayama, Scanning tunneling microscopy and spectroscopy of electron-irradiated thin films of C_{60} molecules, Carbon 49 (6) (2011) 1829–1833. doi:10.1016/j.carbon.2011.01.004.

[33] M. Krause, D. Deutsch, P. Janda, L. Kavan, L. Dunsch, Electrochemical nanostructuring of fullerene films–spectroscopic evidence for C_{60} polymer formation and hydrogenation, Phys. Chem. Chem. Phys. 7 (17) (2005) 3179–3184. doi:10.1039/B504528B.

[34] Y. B. Zhao, D. M. Poirier, R. J. Pechman, J. H. Weaver, Electron stimulated polymerization of solid C_{60}, Appl. Phys. Lett. 64 (5) (1994) 577–579. doi:10.1063/1.111113.

[35] H. Yamawaki, M. Yoshida, Y. Kakudate, S. Usuba, H. Yokoi, S. Fujiwara, et al., Infrared study of vibrational property and polymerization

of fullerene C_{60} and C_{70} under pressure, J. Phys. Chem. 97 (43) (1993) 11161–11163. doi:10.1021/j100145a007.

[36] N. Takahashi, H. Dock, N. Matsuzawa, M. Ata, Plasma-polymerized C_{60}/C_{70} mixture films: Electric conductivity and structure, J. Appl. Phys. 74 (9) (1993) 5790–5798. doi:10.1063/1.354199.

[37] R. Nouchi, K. Masunari, T. Ohta, Y. Kubozono, Y. Iwasa, Ring of C_{60} polymers formed by electron or hole injection from a scanning tunneling microscope tip, Phys. Rev. Lett. 97 (19) (2006) 196101. doi:10.1103/PhysRevLett.97.196101.

[38] E. F. Sheka, Donor-acceptor interaction and fullerene C_{60} dimerization, Chem. Phys. Lett. 438 (1) (2007) 119–126. doi:10.1016/j.cplett.2007.02.053.

[39] E. F. Sheka, Donor-acceptor origin of fullerene C_{60} dimerization, Int. J. Quantum Chem. 107 (13) (2007) 2361–2371. doi:10.1002/qua.21420.

[40] R. Foster, Organic charge-transfer complexes, Vol. 15 of Organic chemistry; a series of monographs, Academic Press, London, 1969.

[41] W. Kohn, Nobel lecture: Electronic structure of matter—wave functions and density functionals, Rev. Mod. Phys. 71 (5) (1999) 1253–1266. doi:10.1103/RevModPhys.71.1253.

[42] P. Hohenberg, W. Kohn, Inhomogeneous electron gas, Phys. Rev. 136 (3B) (1964) B864–B871. doi:10.1103/PhysRev.136.B864.

[43] W. Kohn, L. J. Sham, Self-consistent equations including exchange and correlation effects, Phys. Rev. 140 (4A) (1965) A1133–A1138. doi:10.1103/PhysRev.140.A1133.

[44] K. Lee, E. D. Murray, L. Kong, B. I. Lundqvist, D. C. Langreth, Higher-accuracy van der Waals density functional, Phys. Rev. B: Condens. Matter Mater. Phys. 82 (8) (2010) 081101. doi:10.1103/PhysRevB.82.081101.

[45] J. Klimeš, D. R. Bowler, A. Michaelides, Van der Waals density functionals applied to solids, Phys. Rev. B: Condens. Matter Mater. Phys. 83 (19) (2011) 195131. doi:10.1103/PhysRevB.83.195131.

[46] J. Klimeš, D. R. Bowler, A. Michaelides, Chemical accuracy for the van der waals density functional, J. Phys.: Condens. Matter 22 (2) (2009) 022201. doi:10.1088/0953-8984/22/2/022201.

[47] M. Dion, H. Rydberg, E. Schröder, D. C. Langreth, B. I. Lundqvist, Van der Waals density functional for general geometries, Phys. Rev. Lett. 92 (24) (2004) 246401. doi:10.1103/PhysRevLett.92.246401.

[48] H. Rydberg, M. Dion, N. Jacobson, E. Schröder, P. Hyldgaard, S. I. Simak, et al., Van der Waals density functional for layered structures, Phys. Rev. Lett. 91 (12) (2003) 126402. doi:10.1103/PhysRevLett.91.126402.

[49] M. Dion, van der Waals forces in density functional theory, Ph.D. thesis, Rutgers University (2004).

[50] G. Kresse, J. Furthmüller, Efficient iterative schemes for ab initio total-energy calculations using a plane-wave basis set, Phys. Rev. B: Condens. Matter Mater. Phys. 54 (16) (1996) 11169–11186. doi:10.1103/PhysRevB.54.11169.

[51] G. Kresse, J. Hafner, *Ab initio* molecular-dynamics simulation of the liquid-metal–amorphous-semiconductor transition in germanium, Phys. Rev. B: Condens. Matter Mater. Phys. 49 (20) (1994) 14251–14269. doi:10.1103/PhysRevB.49.14251.

[52] G. Kresse, J. Hafner, *Ab initio* molecular dynamics for liquid metals, Phys. Rev. B: Condens. Matter Mater. Phys. 47 (1993) 558–561. doi:10.1103/PhysRevB.47.558.

[53] G. Kresse, J. Furthmüller, Efficiency of ab-initio total energy calculations for metals and semiconductors using a plane-wave basis set, Comput. Mater. Sci. 6 (1) (1996) 15–50. doi:10.1016/0927-0256(96)00008-0.

[54] P. E. Blöchl, Projector augmented-wave method, Phys. Rev. B: Condens. Matter Mater. Phys. 50 (24) (1994) 17953–17979. doi:10.1103/PhysRevB.50.17953.

[55] G. Kresse, D. Joubert, From ultrasoft pseudopotentials to the projector augmented-wave method, Phys. Rev. B: Condens. Matter Mater. Phys. 59 (3) (1999) 1758–1775. doi:10.1103/PhysRevB.59.1758.

[56] J. P. Perdew, K. Burke, M. Ernzerhof, Generalized gradient approx-

imation made simple, Phys. Rev. Lett. 77 (18) (1996) 3865–3868. doi:10.1103/PhysRevLett.77.3865.

[57] J. P. Perdew, K. Burke, M. Ernzerhof, Generalized gradient approximation made simple [Phys. Rev. Lett. 77, 3865 (1996)], Phys. Rev. Lett. 78 (7) (1997) 1396–1396. doi:10.1103/PhysRevLett.78.1396.

[58] I. Hamada, van der Waals density functional made accurate, Phys. Rev. B: Condens. Matter Mater. Phys. 89 (12) (2014) 121103. doi:10.1103/PhysRevB.89.121103.

[59] I. Hamada, Erratum: van der Waals density functional made accurate [Phys. Rev. B 89, 121103(R) (2014)], Phys. Rev. B: Condens. Matter Mater. Phys. 91 (11) (2015) 119902. doi:10.1103/PhysRevB.91.119902.

[60] K. Hirose, T. Ono, Y. Fujimoto, S. Tsukamoto, First-Principles Calculations in Real-Space Formalism, Imperial College Press, London, 2005.

[61] T. Ono, M. Heide, N. Atodiresei, P. Baumeister, S. Tsukamoto, S. Blügel, Real-space electronic structure calculations with full-potential all-electron precision for transition metals, Phys. Rev. B: Condens. Matter Mater. Phys. 82 (20) (2010) 205115. doi:10.1103/PhysRevB.82.205115.

[62] T. Ono, K. Hirose, Real-space electronic-structure calculations with a time-saving double-grid technique, Phys. Rev. B: Condens. Matter Mater. Phys. 72 (8) (2005) 085115. doi:10.1103/PhysRevB.72.085115.

[63] T. Ono, K. Hirose, Timesaving double-grid method for real-space electronic-structure calculations, Phys. Rev. Lett. 82 (25) (1999) 5016–5019. doi:10.1103/PhysRevLett.82.5016.

[64] J. R. Chelikowsky, N. Troullier, K. Wu, Y. Saad, Higher-order finite-difference pseudopotential method: An application to diatomic molecules, Phys. Rev. B: Condens. Matter Mater. Phys. 50 (16) (1994) 11355–11364. doi:10.1103/PhysRevB.50.11355.

[65] J. R. Chelikowsky, N. Troullier, Y. Saad, Finite-difference-pseudopotential method: Electronic structure calculations without a basis, Phys. Rev. Lett. 72 (8) (1994) 1240–1243. doi:10.1103/PhysRevLett.72.1240.

[66] P. Lazić, N. Atodiresei, M. Alaei, V. Caciuc, S. Blügel, R. Brako, JuNoLo–Jülich nonlocal code for parallel post-processing evaluation of vdW-DF correlation energy, Comput. Phys. Commun. 181 (2) (2010) 371–379. doi:10.1016/j.cpc.2009.09.016.

[67] M. Nakaya, T. Nakayama, Y. Kuwahara, M. Aono, Fabrication of nanostructures by selective growth of C_{60} and Si on Si(111) substrate, Surf. Sci. 600 (13) (2006) 2810–2816. doi:10.1016/j.susc.2006.05.009.

[68] S. Tsukamoto, T. Nakayama, M. Aono, First-principles study on electronic responses of a C_{60} molecule to external electric fields, Chem. Phys. 342 (1–3) (2007) 135–140. doi:10.1016/j.chemphys.2007.09.043.

[69] I. Battisti, V. Fedoseev, K. M. Bastiaans, A. de la Torre, R. S. Perry, F. Baumberger, et al., Poor electronic screening in lightly doped mott

insulators observed with scanning tunneling microscopy, Phys. Rev. B 95 (23) (2017) 235141. doi:10.1103/PhysRevB.95.235141.

[70] M. Weimer, J. Kramar, J. D. Baldeschwieler, Band bending and the apparent barrier height in scanning tunneling microscopy, Phys. Rev. B: Condens. Matter Mater. Phys. 39 (8) (1989) 5572–5575. doi:10.1103/PhysRevB.39.5572.

[71] R. M. Feenstra, Y. Dong, M. P. Semtsiv, W. T. Masselink, Influence of tip-induced band bending on tunnelling spectra of semiconductor surfaces, Nanotechnology 18 (4) (2006) 044015. doi:10.1088/0957-4484/18/4/044015.

[72] D.-L. Huang, P. D. Dau, H.-T. Liu, L.-S. Wang, High-resolution photoelectron imaging of cold C_{60}^- anions and accurate determination of the electron affinity of C_{60}, J. Chem. Phys. 140 (22) (2014) 224315. doi:10.1063/1.4881421.

[73] C. Brink, L. Andersen, P. Hvelplund, D. Mathur, J. Voldstad, Laser photodetachment of C_{60}^- and C_{70}^- ions cooled in a storage ring, Chem. Phys. Lett. 233 (1) (1995) 52–56. doi:10.1016/0009-2614(94)01413-P.

[74] J. de Vries, H. Steger, B. Kamke, C. Menzel, B. Weisser, W. Kamke, et al., Single-photon ionization of C_{60}- and C_{70}-fullerene with synchrotron radiation: determination of the ionization potential of C_{60}, Chem. Phys. Lett. 188 (3–4) (1992) 159–162. doi:10.1016/0009-2614(92)90001-4.

[75] X. Qian, P. Umari, N. Marzari, First-principles investigation of organic photovoltaic materials C_{60}, C_{70}, [C_{60}]PCBM, and bis-[C_{60}]PCBM using a many-body G_0W_0-lanczos approach, Phys. Rev. B: Condens. Matter Mater. Phys. 91 (24) (2015) 245105. doi:10.1103/PhysRevB.91.245105.

[76] H. Zettergren, M. Alcamí, F. Martín, First- and second-electron affinities of C_{60} and C_{70} isomers, Phys. Rev. A 76 (4) (2007) 043205. doi:10.1103/PhysRevA.76.043205.

[77] G. Seifert, R. Gutierrez, R. Schmidt, Ionization energies and coulomb explosion of highly charged C_{60}, Phys. Lett. A 211 (6) (1996) 357–362. doi:10.1016/0375-9601(96)00020-5.

[78] H. Sun, S. Ryno, C. Zhong, M. K. Ravva, Z. Sun, T. Körzdörfer, et al., Ionization energies, electron affinities, and polarization energies of organic molecular crystals: Quantitative estimations from a polarizable continuum model (PCM)-tuned range-separated density functional approach, J. Chem. Theory Comput. 12 (6) (2016) 2906–2916. doi:10.1021/acs.jctc.6b00225.